Germ cell tumors in male patients without gonadal involvement: computed tomography/magnetic resonance imaging findings and diagnostic workflow

Serena Dell'Aversana[1#], Milena Coppola[1#], Valeria Romeo[1], Lorenzo Ugga[1], Luisa Piccin[2], Cesare Sirignano[3], Alessandra D'Amico[1], Ernesto Soscia[3], Elide Matano[2], Francesco Paolo D'Armiento[1], Marialaura Del Basso De Caro[1], Luigi Camera[1], Simone Maurea[1]

[1]Department of Advanced Biomedical Sciences, [2]Department of Clinical Medicine and Surgery, Oncology Division, University of Naples Federico II, Naples, Italy; [3]Institute of Biostructures and Bioimaging of the National Research Council (CNR), Naples, Italy

[#]These authors equally contributed to this work.

Correspondence to: Valeria Romeo, MD, PhD. Department of Advanced Biomedical Sciences, University of Naples Federico II, Via S. Pansini, 5, 80123, Naples, Italy. Email: valeria.romeo@unina.it.

Introduction

Extragonadal germ cell tumors (EGCTs) represent 1% to 5% of all germ cell tumors (GCTs) (1). Morphological type includes mature/immature teratoma, seminoma, yolk sac tumor, embryonal carcinoma, choriocarcinoma and mixed gonadal GCTs. Their anatomic distribution varies widely and includes the mediastinum, sacrococcygeal region, neck, retroperitoneum and other rare anatomic sites. Diagnosis of EGCTs is made on the basis of histological findings and excluding the presence of a testicular/ovarian involvement. Laboratory is pivotal for diagnosis of EGCTs, often demonstrating high levels of human chorionic gonadotropin (β-HCG) and/or α-fetoprotein (α-FP). The prognosis of patients with EGCTs is variable for the possible occurrence of aggressive behavior and distant metastasis (2).

We describe computed tomography (CT) and magnetic resonance (MR) imaging findings of EGCTs reporting a case series of three male patients with different disease's locations that underwent contrast-enhanced CT with or without positron emission tomography (PET) and/or MR examinations. The diagnostic workflow of all patients is also illustrated.

Case presentation

Case 1

A 43-year-old West African male (patient 1) with chronic hepatitis B virus infection was admitted to our hospital to investigate persistent fever, abdominal pain and lung nodular opacities found at previous chest X-ray. Laboratory tests revealed elevated levels of transaminase (AST: 66 U/L, n.v.: 0–34), gamma glutamyl transferase (GGT: 268 U/L, n.v.: 12–64), alkaline phosphatase (ALP: 198 U/L, n.v.: 0–55), and D-lactate dehydrogenase (LDH: 1,018 U/L, n.v.: 125–243). Whole-body contrast-enhanced CT demonstrated the presence of a large mass (15×12 cm^2) in the left sub-phrenic space also involving the left hepatic lobe; enlarged, coarse peritoneal and retroperitoneal lymph-nodes with associated ascites, carcinomatous solid nodules as well as bone, liver and lung metastases were also found (*Figure 1*). A subsequent contrast-enhanced MR examination confirmed all CT findings, showing the presence of a heterogeneous hypervascular tumoral mass with restricted diffusion involving the left hepatic lobe, pancreatic head as well as gastric antrum and duodenum. Large abdomino-pelvic ascites and neoplastic occlusion
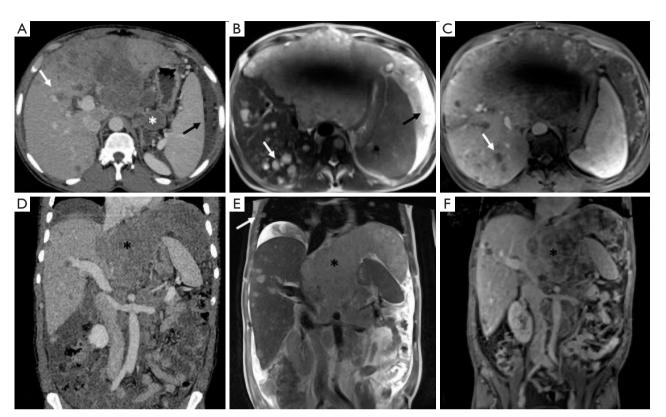
Figure 1 Patient 1. Axial (A) and coronal reformatted (B) contrast-enhanced CT images in the portal phase; axial (C) and coronal (D) Turbo Spin Echo T2-weighted images; axial (E) and coronal (F) contrast-enhanced VIBE T1-weighted images acquired in the portal phase. Multiple hepatic metastases (white arrows), peritoneal solid nodules (white asterisk) as well as ascite are appreciated. A large, heterogeneous tumor mass is also detectable in the left sub-phrenic space involving the left hepatic lobe (black asterisks).

of the left portal branch were also observed. On the basis of imaging findings, a diagnostic hypothesis of metastatic mesenchymal tumor was formulated. However, further laboratory examinations showed a significant increase of α-FP (>3,000 ng/mL, n.v.: 0–15) and β-HCG (27 mIU/mL, n.v.: <5) and biopsy of the left hepatic lobe was suggestive of non-seminomatous germ cell tumor (GCT) infiltration. Ultrasound (US) examination ruled out the presence of a primary testicular tumor. After consulting with the interdisciplinary tumor board, the patient was treated with a chemotherapy protocol consisting of first cycle of cis-Platin and Etoposide followed by three cycles of Bleomycin, Etoposide and cis-Platin (BEP), showing a significant reduction (>50%) in tumor size at CT images right after the first cycle of treatment. A CT scan was performed right after the first cycle according as chosen by the oncologists in order to exclude progression disease as patient's clinical status worsened, probably due to chemotherapy toxicity. However, despite the documented response to treatment

and probably due to the advanced stage of the disease, the patient died after 5 months of chemotherapy.

Case 2

A 23-year-old Caucasian male (patient 2) was admitted to our department to investigate acute abdominal pain. Laboratory values were normal. US examination showed the presence of a retroperitoneal hypoechoic mass with abnormal vascularization by color-Doppler US imaging; on the basis of sonographic findings, a diagnostic hypothesis of sarcoma was formulated. Contrast-enhanced CT scan was then performed confirming the presence of the heterogeneous hypervascular retroperitoneal mass, measuring 88×48 mm^2 on axial plane with longitudinal extension of 130 mm, located in the right paraaortic space, compressing the inferior vena cava and determining anterior dislocation of the duodenum; CT images also showed the presence of heterogeneously vascularized

2002

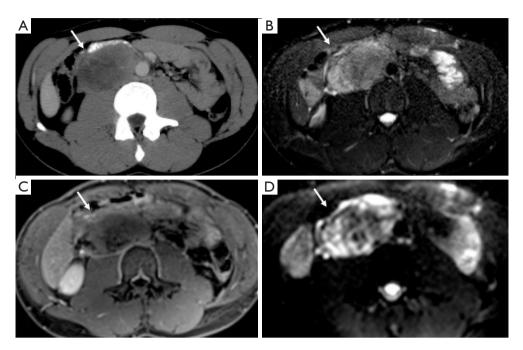Dell'Aversana et al. Integrated imaging of extragonadal germ cell tumors

Figure 2 Patient 2. (A) Axial contrast-enhanced CT image obtained in the portal phase; (B) axial Turbo Spin Echo T2-weighted image with fat suppression; (C) axial contrast-enhanced VIBE T1-weighted image; (D) axial diffusion weighed image (b800). A heterogeneous hypervascular retroperitoneal mass, with restricted diffusivity, is detected in the right paraaortic space (white arrows), compressing the inferior vena cava.

hepatic nodules at V, VI and VII segments. Contrast-enhanced MR examination was also performed confirming the malignant features of the mass since heterogeneous T2 signal intensity, hypervascularity and restricted diffusion were observed; MR also confirmed the presence of multiple hepatic nodules, hyperintense on T2-weighted images, hypervascularized on dynamic post-contrast sequences and with restricted diffusion on diffusion weighted imaging (DWI), suspicious for metastases. CT and MRI findings of retroperitoneal mass and hepatic nodules are illustrated in *Figures 2,3*, respectively. Further laboratory tests showed high levels (11,991 ng/mL; n.v.: 0–15 ng/mL) of α-FP. Biopsy confirmed the diagnosis of a non-seminomatous EGCTs. No testicular lesions were found at US examination. After consulting with the interdisciplinary tumor board, the patient was treated with four cycles of chemotherapy (BEP). Follow-up contrast enhanced 2-(^{18}F) fluoro-2-deoxy-d-glucose [2-(^{18}F)FDG] PET/CT scans performed during and right after first cycle of treatment, showed a progressive significant reduction of tumor size (>50% and 40% respectively) and tracer uptake with a maximum standard uptake volume (SUVmax) of 6.2 and 3.3, respectively; hepatic metastases were also significantly

reduced in size and did not show tracer uptake. The residual tumor resection was not performed due to the close relationship of the mass with the inferior vena cava and considering the good response to chemotherapy. The patient has been in follow-up for 2 years.

Case 3

A 23-year-old man (patient 3) came to our department for a progressive worsening of right hemiplegia, previously ascribed to cerebrovascular disease, and onset of insipid diabetes. The patient underwent brain contrast-enhanced MR which depicted a left basal ganglia lesion also involving thalamus, corona radiata, deep temporal white matter and corpus callosum. The lesion showed inhomogeneous signal intensity, with cystic and hemorrhagic components, and moderate enhancement. Perfusion weighted imaging demonstrated high cerebral blood volume values within the lesion while decreased values were revealed at the left hemispheric cortex, with ipsilateral atrophy on conventional sequences. A second MR examination, performed after clinical worsening, showed a wide perivascular spread of the pathology for which a lymphoma was suspected (*Figure 4*).
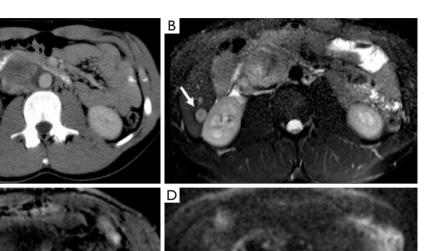
Figure 3 Patient 2. (A) Axial contrast-enhanced CT image obtained in the portal phase; (B) axial Turbo Spin Echo T2-weighted image with fat suppression; (C) axial contrast-enhanced VIBE T1-weighted image acquired in the portal phase; (D) axial diffusion weighted image (b800). In the same case reported in *Figure 2*, hypovascular hepatic nodules (white arrows in A and C), hyperintense in fat-sat T2w (white arrow in B) and DWI images (white arrow in D) are detected.

To confirm this hypothesis the patient underwent a stereotaxic biopsy whose findings were consistent with a non-seminomatous GCT. Testes were found free from primary tumor lesions at US examination. Laboratory values for cancer markers were normal. After consulting with the interdisciplinary tumor board, the patient underwent radiotherapy showing a volume reduction greater than 50% at MR examination; subsequently four cycles of chemotherapy (cis-Platin, Cytarabine and Rituximab) were practiced. Residual tumor resection was not considered due to the large extension of the mass. The patient has been in follow-up for 2 years. A summary of clinical and imaging findings for all cases is reported in *Table 1*.

Discussion

EGCTs represent 1–5% of all GCTs (1) and are usually seen in children or young male adults. In adults, most common sites of primary extragonadal germ cell tumors (EGCTs) are, in descending order, the mediastinum (15%), retroperitoneum (10% of all primary malignant retroperitoneal tumors), and cranium. In children, the skull and sacrococcygeal region are common sites (3).

Abdominal and low back pain are the most frequent symptoms, as pain can simulate a renal colic. Other clinical symptoms and signs include a palpable mass, weight loss, constipation, hip and back pain, dyspnea, leg edema, fever, varicocele, and urinary retention (4,5). EGCTs are morphologically similar to gonadal GCTs and most often occur in the midline, depending on a migration defect of primordial germ cells (6,7). EGCTs are the result of a malignant transformation of misplaced germ cells and histological features depend on their development stages and microenvironment. A different hypothesis is that EGCTs may represent metastatic lesions of a testicular/ ovarian tumor primary occult or undergoing involution ("burned out") (8). We describe CT and MR imaging findings of EGCTs reporting three cases of male patients. In detail, patient 1 presented a rare, diffuse infiltrating pattern located in both peritoneal and retroperitoneal space with also thoracic, liver and bone involvement, as also occur in the 35% of patients with EGCTs (9). In this case, the widespread involvement of different anatomical districts with mediastinal sparing which is, instead, a common site of EGCTs localization (10), made it difficult to hypothesize a primary origin. A

2004

Dell'Aversana et al. Integrated imaging of extragonadal germ cell tumors
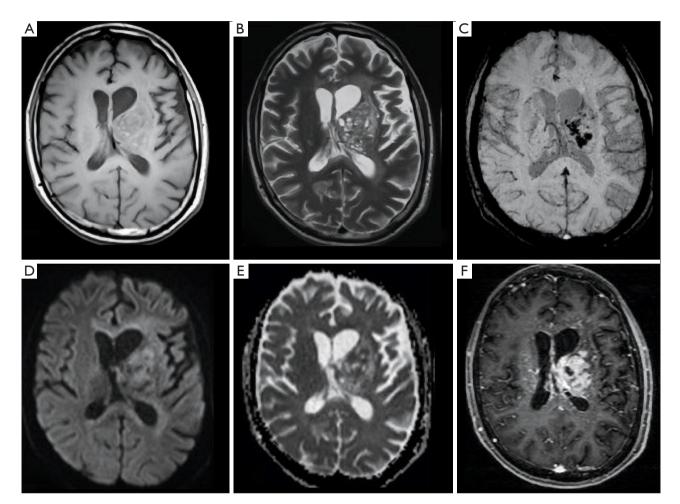
Figure 4 Patient 3. Axial Spin Echo T1-weighted (A), Turbo Spin Echo T2-weighted (B), susceptibility weighted (C), diffusion weighted (b1000 and ADC map, D,E) and Turbo Field Echo T1-weighted after contrast administration (F) images. A left basal ganglia lesion also involving thalamus, corona radiata, deep temporal white matter and corpus callosum is appreciated. The lesion showed inhomogeneous signal intensity, with cystic and hemorrhagic components, and moderate enhancement.

suspicion of mesenchymal tumor was made, mainly on the basis of the diffuse peritoneal involvement. Patient 2 showed an isolated large mass in the right paraaortic space with hepatic metastasis; in this case, soft-tissue sarcoma was first hypothesized. Primary retroperitoneal GCTs occur in about 10% of malignant retroperitoneal tumors and 30–40% of EGCTs. These lesions are usually large at diagnosis, often presenting at imaging as masses determining encasement, displacement and compression of abdominal vessels (9). Of note, there are no definite imaging features that can help in distinguishing primary retroperitoneal EGCTs from lymphoma, thymic neoplasms, metastatic lymph nodes, neurogenic tumor or retroperitoneal soft-tissue sarcoma (9).

Patient 3 presented a rare brain localization within basal ganglia, thalamus, corona radiata, deep temporal region and corpus callosum involvement, and lymphoma was initially hypothesized; in particular, there was no involvement of the pineal gland and suprasellar region, which are the most frequent intracranial sites of EGCTs. Indeed, basal ganglia and thalamus are primarily involved in about 10% of cases (11). These EGCT show a growth rate higher than pineal and suprasellar counterpart, with possible cysts and hemorrhage. Ectopic basal ganglia EGCT can also present mild hyperintensity on T1-weighted images, due to iron and manganese depositions (12). Hemispheric cerebral atrophy is reported in about 20% of cases caused by Wallerian

Table 1 Summary of clinical and imaging features

Features	Case 1	Case 2	Case 3
Symptoms	Persistent fever, abdominal pain	Acute abdominal pain	Right hemiplegia
Laboratory	• α-FP >3,000 ng/mL, (n.v.: 0–15) • β-HCG 27 mIU/mL, (n.v.: <5)	• α-FP =11,991 ng/mL; n.v.: [0–15]	Normal
Location	• Peritoneal space • Retroperitoneal space • Thorax • Liver • Bone	• Right paraaortic space	• Left basal ganglia • Thalamus • Corona radiata • Deep temporal white matter • Corpus callosum
CT-PET/CT	• Heterogeneous, hypervascular mass in the left sub-phrenic space involving the left hepatic lobe • Enlarged, coarse peritoneal and retroperitoneal lymph-nodes • Ascites • Carcinomatous solid nodules • Bone, liver and lung metastasis	• Heterogeneous hypervascular retroperitoneal mass • High 2-(^{18}F)FDG uptake at first follow-up PET/CT scan (SUVmax 6.2), significantly reduced after treatment (3.3)	–
MR	• Heterogeneous, hypervascular mass with restricted diffusion in the left sub-phrenic space involving the left hepatic lobe • Enlarged, coarse peritoneal and retroperitoneal lymph-nodes • Ascites • Carcinomatous solid nodules • Bone, liver and lung metastasis (partially visualizes)	• Heterogeneous T2 signal intensity, hypervascularity and restricted diffusion	• Inhomogeneous signal intensity, for cystic and hemorrhagic components, moderate enhancement with high cerebral blood volume values at PWI
Treatment	BEP	BEP	Radiotherapy
Outcome	Exitus	Partial response	Partial response

α-FP, α-fetoprotein; β-HCG, human chorionic gonadotropin; CT, computed tomography; PET, positron emission tomography; 2-(^{18}F) FDG, 2-(^{18}F)fluoro-2-deoxy-d-glucose; SUVmax, maximum standard uptake volume; MR, magnetic resonance; PWI, perfusion weighted imaging; BEP, bleomicine etoposide and cisplatin.

degeneration (13). In all cases final diagnosis of primitive EGCTs was obtained by means of biopsy integrated by tumor/laboratory markers, a US examination negative for testicular abnormalities and good response to therapy; imaging features of EGCTs are unspecific, thus the definitive diagnosis requires biopsy and integration with laboratory.

Several cases of EGCTs in male patients have been previously described. Routh *et al.* reported a case of retroperitoneal EGCTs presenting as a large

heterogeneously vascularized on CT images, extending across the midline, behind the duodenum, against the pancreas and overlying the inferior vena cava (14). A case of an anterior mediastinal mass with aorto-pulmonary window and left paracardiac invasion, showing high FDG uptake was also described (15). A series of eight cases of EGCTs, of which 5 mediastinal and 3 retroperitoneal, was reported by Medini and colleagues (10). According to the literature, EGCTs often present as bulky, heterogeneously vascularized masses with irregular margins on imaging

studies; in particular, CT as well as MR imaging features may vary depending on the presence of cystic, fat, hemorrhagic and necrotic content (9). Primary intracranial EGCTs usually present as discrete homogeneous enhancing masses, with cystic component; the signal intensity of the solid component is similar to that of gray matter and invasion of adjacent structures is common (16). Imaging findings are often unspecific, as also occurred in our case series, and therefore not helpful to characterize tumor lesions; on the other hand, laboratory markers (α-FP, β-HCG and LDH) may aid to hypothesize EGCTs (17,18) and can also be used during the follow-up. Even if limited for diagnosis, imaging modalities play an important role for the staging in assessing tumor extent and adjacent organ involvement, mainly using CT, often along with [2-(^{18}F) FDG] PET-CT (19); moreover, [2-(^{18}F)FDG] PET-CT has a main role in the detection of viable tumor in the residual mass after chemotherapy (20). MR imaging, also integrated with metabolic [2-(^{18}F)FDG] scan, could give more tissue information to further characterize tumor masses and could be also useful during the follow-up of young patients avoiding radiation exposure (21-23).

In conclusion, in case of atypical imaging findings suspected of malignancy in young adults, ECGTs should be considered in the differential diagnosis and whole-body tomographic imaging always performed, integrated with laboratory data. Since anatomical sites of malignancy are unpredictable, we suggest to perform a preliminary whole-body CT imaging followed by MR of the involved anatomical districts. Integrated metabolic imaging such as whole-body PET-CT or PET-MR may also be considered when functional evaluation of tumor lesions may be useful for diagnosis or follow-up.

Acknowledgments

Footnote

Conflicts of Interest: The authors have no conflicts of interest to declare.

References

1. McKenney JK, Heerema-McKenney A, Rouse RV. Extragonadal germ cell tumors: a review with emphasis on pathologic features, clinical prognostic variables, and differential diagnostic considerations. Adv Anat Pathol 2007;14:69-92.

2. Makino T, Konaka H, Namiki M. Clinical Features and Treatment Outcomes in Patients with Extragonadal Germ Cell Tumors: A Single-center Experience. Anticancer Res 2016;36:313-7.

3. Ueno T, Tanaka YO, Nagata M, Tsunoda H, Anno I, Ishikawa S, Kawai K, Itai Y. Spectrum of Germ Cell Tumors: From Head to Toe. Radiographics 2004;24:387-404.

4. Rosado-de-Christenson ML, Templeton PA, Moran CA. Mediastinal germ cell tumors: radiologic and pathologic correlation. RadioGraphics 1992;12:1013-30.

5. Nichols CR. Mediastinal germ cell tumors: clinical features and biologic correlates. Chest 1991;99:472-9.

6. Schmoll HJ. Extragonadal germ cell tumors. Ann Oncol 2002;13:265-72.

7. Oosterhuis JW, Stoop H, Honecker F, Looijenga LH. Why human extragonadal germ cell tumors occur in the midline of the body: old concepts, new perspectives. Int J Androl 2007;30:256-63.

8. Hainsworth JD, Greco FA. Extragonadal germ cell tumors and unrecognized germ cell tumors. Semin Oncol 1992;19:119-27.

9. Shinagare AB, Jagannathan JP, Ramaiya NH, Hall MN, Van den Abbeele AD. Adult extragonadal germ cell tumors. AJR Am J Roentgenol 2010;195:W274-80.

10. Medini E, Levitt SH, Jones TK, Tao Y. The management of extratesticular seminoma without gonadal involvement. Cancer 1979;44:2032-8.

11. Tamaki N, Lin T, Shirataki K, Hosoda K, Kurata H, Matsumoto S, Ito H. Germ cell tumors of the thalamus and the basal ganglia. Childs Nerv Syst 1990;6:3-7.

12. Rasalkar DD, Chu WC, Cheng FW, Paunipagar BK, Shing MK, Li CK. Atypical location of germinoma in basal ganglia in adolescents: radiological features and treatment outcomes. Br J Radiol 2010;83:261-7.

13. Kim CH, Paek SH, Park IA, Chi JG, Kim DG. Cerebral germinoma with hemiatrophy of the brain: report of three cases. Acta Neurochir (Wien) 2002;144:145-50; discussion 150.

14. Routh A, Hickman BT, Smith EE. Retroperitoneal seminoma. CA Cancer J Clin 1982;32:78-81.

15. Saba L. The primitive extratesticular seminoma: diagnosis of a rare pathology. Acta Biomed 2017;88:82-5.

16. Liang L, Korogi Y, Sugahara T, Ikushima I, Shigematsu Y, Okuda T, Takahashi M, Kochi M, Ushio Y. MRI of intracranial germ-cell tumours. Neuroradiology

2002;44:382-8.

17. Busch J, Seidel C, Zengerling F. Male Extragonadal Germ Cell Tumors of the Adult. Oncol Res Treat 2016;39:140-4.

18. Gilligan TD, Seidenfeld J, Basch EM, Einhorn LH, Fancher T, Smith DC, Stephenson AJ, Vaughn DJ, Cosby R, Hayes DF; American Society of Clinical Oncology. American Society of Clinical Oncology Clinical Practice Guideline on uses of serum tumor markers in adult males with germ cell tumors. J Clin Oncol 2010;28:3388-404.

19. Romeo V, Esposito A, Maurea S, Camera L, Mainenti PP, Palmieri G, Buonerba C, Salvatore M. Correlative Imaging in a Patient with Cystic Thymoma: CT, MR and PET/CT Comparison. Pol J Radiol 2015;80:22-6.

20. Cremerius U, Effert PJ, Adam G, Sabri O, Zimmy M, Wagenknecht G, Jakse G, Buell U. FDG PET for detection and therapy control of metastatic germ cell tumor. J Nucl Med 1998;39:815-22.

21. Kvammen Ø, Myklebust TÅ, Solberg A, Møller B, Klepp OH, Fosså SD, Tandstad T. Long-term Relative Survival after Diagnosis of Testicular Germ Cell Tumor. Cancer Epidemiol Biomarkers Prev 2016;25:773-9.

22. Romeo V, Esposito A, Maurea S, Camera L, Mainenti PP, Palmieri G, Buonerba C, Salvatore M. Correlative Imaging in a Patient with Cystic Thymoma: CT, MR and PET/CT Comparison. Pol J Radiol 2015;80:22-6.

23. Nensa F, Beiderwellen K, Heusch P, Wetter A. Clinical applications of PET/MRI: current status and future perspectives. Diagn Interv Radiol 2014;20:438-47.